Membrane-Based Functions in the Origin of Cellular Life

Final Technical Report for Contract NCC2-772

Christophe Chipot[a], Michael H. New[b], Karl Schweighofer[b,c], Andrew Pohorille[b,c], and Michael A. Wilson[b,c]

[a]Laboratoire de Chimie Théorique, Unité Mixte de Recherche CNRS 7565, Université Henri Poincaré - Nancy I, B.P. 239, 54506 Vandœuvre-lès-Nancy, France
[b]Dept. Pharmaceutical Chemistry, University of California, San Francisco, 94143
[c]Exobiology Branch, NASA Ames Research Center, Moffett Field, CA 94035

Period of Performance: October 1, 1995 - March 31, 1999

Inventions: There are no patents or inventions arising from this research project.

Objectives

Our objective is to help explain how the earliest ancestors of contemporary cells (protocells) performed their essential functions employing only the molecules available in the protobiological milieu. Our hypothesis is that vesicles, built of amphiphilic, membrane-forming materials, emerged early in protobiological evolution and served as precursors to protocells. We further assume that the cellular functions associated with contemporary membranes, such as capturing and transducing of energy, signaling, or sequestering organic molecules and ions, evolved in these membrane environments. An alternative hypothesis is that these functions evolved in different environments and were incorporated into membrane-bound structures at some later stage of evolution.

We focus on the application of the fundamental principles of physics and chemistry to determine how they apply to the formation of a primitive, functional cell. Rather than attempting to develop specific models for cellular functions and to identify the origin of the molecules which perform these functions, *our goal is to define the structural and energetic conditions that any successful model must fulfill, therefore providing physico-chemical boundaries for these models.* We do this by carrying out large-scale, molecular level computer simulations on systems of interest.

Specific systems that we have investigated are:

1. Simulations of water-membrane systems to yield an accurate description of the electrical properties of the membranes. This was investigated by calculating the surface potentials of aqueous interfaces and the interaction of a number of small polar and nonpolar solute molecules with several membrane interfaces.

2. Simulations of ion transport across a water-membrane interface to investigate how "thinning" defects in the membrane effectively increase the permeability of the membrane by several orders of magnitude over predictions based on simple, dielectric continuum models.

3. Simulations of small peptides at the water-hexane interface to investigate how the interface affects the structure of the peptide, and in particular if short peptides, which are disordered in water, can fold into ordered structures at the interface.

Summary

Structure of membranes and their permeability to small molecules and ions. Our earlier studies on membranes composed of glycerol 1-monooleate (GMO), which are sufficiently simple to be good models for protobiological membranes, were extended to phospholipid bilayers composed of dipalmitoylphosphatidylcholine (DPPC) and 1-palmitoyl 2-oleoyl sn-glycero 3-phosphocholine (POPC) All these studies show that water readily penetrates the head groups but not the hydrophobic, highly disordered core of the bilayer. The surface of the bilayer undergoes considerable fluctuations which lead to the formation of thinning defects in the membrane. Similar defects provide pathways for unassisted ion transport across membranes. Simple monovalent cations, such as Na^+, move across the membrane well-solvated by water and lipid head groups. The formation of defects increases membrane permeability to ions by 13–15 orders of magnitude, rendering the transport feasible even in the absence of ion channels or carriers.

The water-membrane interface was shown to have the unique property that it concentrates many small solutes that exhibit some degree of polarity but are not necessarily amphiphilic. A general theory of this phenomenon was developed based on the balance between electrostatic and non-electrostatic contributions to the free energy of transferring these solutes across the interface. Explaining how small molecules are distributed in membranes has broad implications for understanding their permeation across protocellular walls, primitive, heterogeneous catalysis and simple, photo-induced charge transfer.

Peptides at membrane interfaces. In analogy with modern proteins, which fold into well-defined structures, we expect that peptides must adopt ordered structures before they can perform various protocellular functions. The ability of small peptides to organize at aqueous interfaces was examined by investigating peptides composed of two amino acids, nonpolar leucine and polar glutamine, but having different sizes and sequences of amino acids. Among them were dipeptides, heptamers designed to maximize the interfacial stability of an α-helix and a β-strand, and an undecamer composed entirely of leucine residues. Using the undecamer of leucine as a model, the complete folding of a peptide from a disordered structure to an α-helix was accomplished for the first time in computer simulations that correctly accounted for solvent effects. These simulations revealed principles governing the organization of peptides at interfaces:

1. Short peptides tend to accumulate at interfaces and acquire ordered structures, providing that they have a proper sequence of polar and nonpolar amino acids. The specific identity of amino acids is less important, a desirable protobiological property. Once folded, the peptides may organize into structures suitable for polymerization or catalytic activity. The interfacial structure of peptides is mainly determined by the

hydrophobic effect, which is manifested at aqueous interfaces as a tendency for polar and nonpolar groups of the solute to segregate into the aqueous and nonpolar phases, respectively.

2. If peptides consist of nonpolar residues only, they partition into the nonpolar phase and simultaneously fold into an α-helix. Once in the nonpolar environment, they can adjust their structure and orientation to changing external conditions. This may have provided a simple mechanism of transmitting signals from the environment to the interior of a protocell.

Introduction

An important step in the origin of life was the organization of material in the prebiotic environment into a protocell, which is a hypothetical precursor of modern cells. A protocell would have been able to sequester material from the external environment, to carry out the chemical reactions necessary to maintain its integrity and allow growth, and to divide (thereby reproducing), possibly in the absence of a genome. Since all known cells have membrane-like barriers separating the interior from the external environment and since all known cells use proteins to catalyze the chemical reactions along their metabolic pathways, we envision a protocell that is formed from a simple, lipid bilayer membrane that uses peptides — short amino acid polymers that are simpler than modern proteins — as primitive catalysts. This model of a protocell forms the basis of the research described herein: how a bilayer membrane, in which hydrophobic and hydrophilic media exist in close proximity, affects the concentration of material in its vicinity and the transport of material across the membrane; and how the membrane can affect the structure of short peptides, stabilizing folded structures such as α-helices and β-strands which have catalytic possibilities as well as the association of these folded peptide subunits into larger structures, such as transmembrane channels.

In analogy with modern proteins, the stability and catalytic properties of peptides will depend upon their ability to adopt well-defined structures. Unfortunately, short peptides are usually disordered in aqueous solutions and therefore, do not appear to be suitable for carrying out these functions. However, many of these peptides can acquire a broad range of well-defined secondary structures, such as α-helices, β-strands or β-turns, at water-membrane, water-oil or water-air interfaces, the precise secondary structure being determined by the sequence of amino acids. A crucial, common characteristic of these interfaces is that a nonpolar phase is adjacent to an aqueous phase. This research project has investigated the properties of these interfaces and its consequences on the equilibrium distribution and conformational and orientational ordering of small solutes and peptides at these interfaces.

In this report, we discuss the interaction of small solutes with membrane interfaces, and show how the structural and electrical properties of the membrane affect the adsorption and conformational equilibria of the solutes. These ideas are then applied through simulations of small peptides at a water-hexane interface. The close proximity of the aqueous and nonpolar phases induce the peptide to adopt conformations that are amphipathic such that the

hydrophilic residues are solvated by the aqueous phase and the hydrophobic residues are solvated by the nonpolar phase. These same principles are shown to govern the folding of a small, hydrophobic peptide at a water-hexane interface and the insertion of this peptide into the hexane phase. We then discuss the unassisted transport of ions across a simple glycolipid membrane. Simple solvation models, based on the different dielectric constants of the membrane interior and the aqueous phase, predict free energy barriers that are several orders of magnitude larger than inferred experimentally. Simulation results show how deformation of the membrane and transport of several solvated water molecules with the ion can lower this free energy barrier to a value consistent with experimental results. Finally, we present some preliminary results on ion channels, which are transmembrane peptide assemblies which allow transport of ions across membranes with a much lower free energy barrier than unassisted transport. For more detailed overviews of this work, please see (Pohorille *et al.*, 1996) and (Pohorille *et al.*, 1999).

Methods

The MD simulations were carried out in the (N,V,E) or (N,p,T) ensembles. In an (N,V,E) ensemble, the number of atoms or molecules, N, in the system are constant and the volume, V, is fixed. The equations of motion for the particles in the system (Newton's equations) are conservative and the total energy, E, is a constant of the motion. In an (N,p,T) ensemble, the volume is allowed to fluctuate around a constant fixed pressure, p, and the energy is allowed to fluctuate under the condition that the temperature of the system is a constant. For example, most simulations are carried out at temperatures close to 300 K and pressures close to 1 atm, which correspond to typical conditions on the contemporary earth. It is under these conditions that most laboratory experiments are carried out. For most systems, the ensemble is chosen as a matter of convenience.

The system consisted of either one or two lamellae of water in contact with either a lamella of hexane or a bilayer membrane consisting of glycerol-1-monooleate (GMO) or 1-palmitoyl 2-oleoyl sn-glycero 3-phosphatidylcholine (POPC), and one solute molecule. The actual system sizes varied, depending upon the the size of the solute molecule.

Simulations in the (N,V,E) ensemble were: a system containing one small solute molecule, such as a methane derivative or small alcohol or alkane, and a lamella 500 water molecules in contact with a lamella of 84 hexane molecules in a simulation box with a cross sectional area of 24 Å × 24 Å; a system containing larger solutes, such as an undecamer of poly-L-leucine, interacting with 1380 water molecules and 409 hexane molecules in a simulation box of 42 Å × 42 Å; a water-GMO membrane system contained two lamella of 1152 water molecules, each, in contact with a lipid bilayer containing 72 GMO molecules in a box with a cross sectional area of 37 Å × 37 Å. Calculations carried out in the (N,p,T) ensemble used 5743 TIP3P (Jorgensen *et al.*, 1983) water and 64 POPC molecules in a simulation box with an average cross section of 51 Å × 40 Å.

Periodic boundary conditions were applied in all three directions. The equation of motions were solved using the Verlet algorithm with time steps of 2 or 2.5 fs. Calculations were performed at either 300 K or 310 K. In all calculations performed in the (N,V,E) systems,

the water was represented using the TIP4P model and the hexane molecules using the the OPLS (Jorgensen *et al.*, 1984; Jorgensen and Tirado-Rives, 1988) model. The hydrocarbon tail of GMO was also represented using the OPLS (Jorgensen *et al.*, 1984; Jorgensen and Tirado-Rives, 1988) model and the head group potentials were derived from quantum mechanical calculations on glycerol. (Wilson and Pohorille, 1994) The potentials for small solutes were developed from quantum mechanical calculations. (Pohorille and Wilson, 1996) The nonbonded and the intramolecular parameters for the peptides were taken from the AMBER force field of Cornell. (Cornell *et al.*, 1995) In the (N,V,E) simulations, the intermolecular interactions involving water molecules and/or small, electrically neutral groups of the solute and hexane molecules were smoothly truncated between 7.5 and 8.0 Å. For the (N,p,T) simulations of a water-POPC bilayer system, the head groups of the phospholipid are zwitterionic, and long-ranged forces were calculated using the Particle Mesh Ewald method. (Essmann *et al.*, 1995)

Results

Properties of Aqueous Interfaces and Adsorption of Small Solutes: Understanding the structure of aqueous interfaces is the first step towards proposing physically motivated, implicit models of these systems. Probably the most direct characteristics of the interface are the mass and atomic density profiles in the direction perpendicular to the interface. The mass density profiles are shown in Fig. 1 and the atomic density profiles for water-octanol and water-POPC systems are shown in Fig. 2. The atomic density profiles for water-hexane and water-GMO interfaces have been published previously. (Wilson and Pohorille, 1994; Pohorille, 1998) In all cases, the origin was set at the equimolar surface of water, defined as the surface where the excess density on the side in contact with the organic phase is balanced by the depletion of density on the bulk water side. As can be seen from Fig. 1, the mass density across the interfaces is not only non-uniform, but also non-monotonic. Furthermore, the profiles are different for different interfaces. As will be argued below, these differences have direct bearing on the excess chemical potential of solutes in the interfacial region.

Although atomic densities of the two phases in contact overlap in all four cases, it does not always imply interpenetration at the molecular level. In fact, simulation results have shown that most liquid-liquid interfaces are locally sharp, but they are broadened by spatial and temporal averaging over fluctuations caused by capillary waves. (Pohorille and Wilson, 1993; Benjamin, 1997) This picture has been borne out by the results of recent scattering experiments on liquid-liquid interfaces. (Mitrinovic *et al.*, 1999; Zhang *et al.*, 1999) In the water-hexane system, dewetting of the nonpolar oily phase produces a small minimum in the mass density profile at the interface. In the water-octanol system, the interface is also locally sharp, but the minimum disappears due to favorable interaction between hydroxyl groups of water and octanol. The additional structure of the profiles for octanol is a result of the interfacially induced, "tail-to-tail" ordering of octanol which persists to some extent for a few molecular layers. In particular, the minimum at approximately 10 Å from the interface corresponds to the region in which tails of oppositely directed layers of octanol molecules

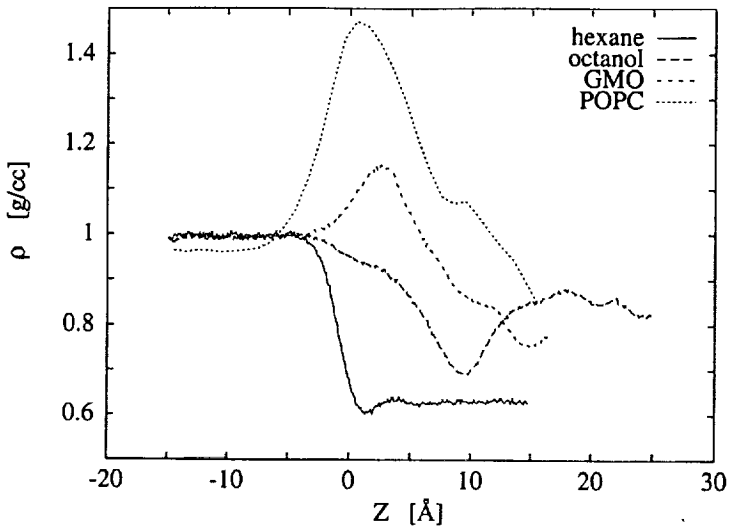

Figure 1: Mass density profiles at the water-hexane, water-octanol, water-GMO and water-POPC interface. The origin is defined by the equimolar surface of water, and the water lies to the left.

are in contact.

In contrast to liquid-liquid interfaces, overlaps in atomic density profiles observed for water-membrane system reflect penetration of water into the lipid head groups. This, in turn, creates a high density interfacial region, especially near very polar POPC head groups. Note, that density profiles for water-POPC system converge on the aqueous side to a slightly different value than the other three profiles because a different model of water was employed in the simulations.

The non-uniform orientational distribution of molecules in the interfacial region generates the electric field, $E_z(z)$, in the z-direction. $E_z(z)$ can be conveniently calculated as: (Wilson *et al.*, 1987)

$$E_z(z) = \frac{2\pi\langle q_-(z) - q_+(z)\rangle}{A}, \tag{1}$$

where $q_+(z)$ and $q_-(z)$ are total charges on both sides of the plane located at height z and A is the xy cross-sectional area of the simulation box.

The average electric fields across the interfaces are shown in Fig. 3. As expected, they disappear in the bulk phases but they are quite large in the interfacial regions. As was the case with the density profiles, the electric fields are non-monotonic and depend upon the nature of the interface. For the water-hexane system, E_z is positive on the water side of the interface, but negative of the hexane side. This reflects the orientational preferences of water molecules in the interfacial region. The most common orientation of water molecules directly in contact with the organic phase is such that one O-H bond points toward the organic liquid whereas the other O-H bond is directed into the aqueous phase.

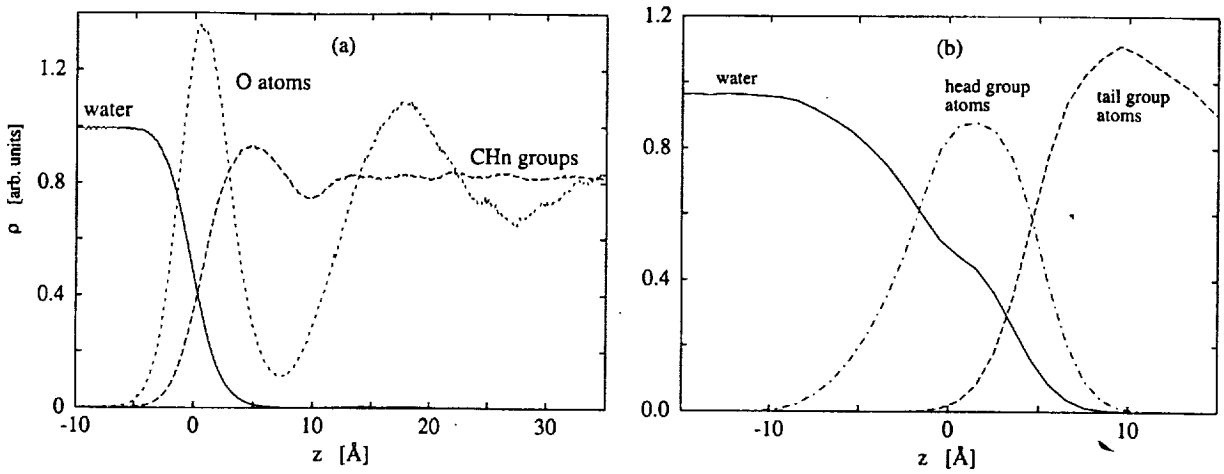

Figure 2: Density profiles of (a) water and octanol O atoms and CH_n groups at the water-octanol interface and (b) water, POPC head group atoms and POPC tail group atoms at the water-POPC interface. The geometry is defined in Fig 1

For the other three interfaces, E_z is a sum of contributions from water and the head groups interacting with the aqueous phase. As a result, the positive peak on the aqueous side of water-octanol and water-GMO systems disappears, whereas the negative peak not only remains in place but becomes deeper. The profile of E_z for water-POPC system is even more complicated. The minimum is shifted towards the aqueous side with respect to the equimolar surface of water due to the increased penetration of water into the POPC head groups. The additional peak on the membrane side reflects the molecular structure and relatively rigid orientation of the head groups.

In general, it may be anticipated that the large interfacial electric fields will influence properties of solutes at interfaces. In particular, it may be expected that they will induce orientational preferences of small dipolar species in the interfacial region. We will show that this is indeed the case.

Calculating the chemical potentials of small solutes. We are concerned with the calculation of the excess chemical potential, $\Delta\mu_{exc}$, of a solute in an interfacial environment. This quantity represents the quasistatic work needed to bring a solute molecule from the gas phase to solution and can be expressed as:

$$\Delta\mu_{exc} = \mu - \mu_{ideal}, \tag{2}$$

where μ and μ_{ideal} are the chemical potentials of the solute in solution and in ideal gas, respectively. In interfacial systems, $\Delta\mu_{exc}$ is a function of the z-coordinate, perpendicular to the interface. However, since this dependence has no influence on the derivations presented below, we will omit it to simplify notation.

A very efficient method for estimating $\Delta\mu_{exc}$ of small solutes is provided by the potential distribution theorem. (Widom, 1963; Widom, 1982) In this method, only the system *without*

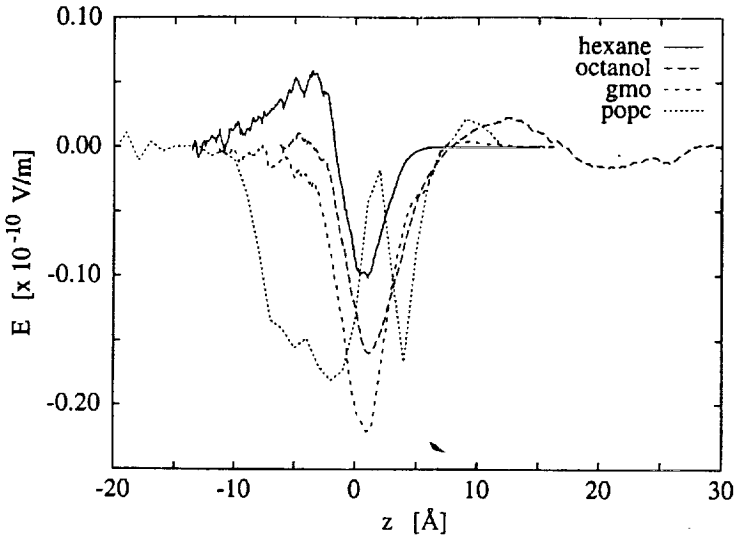

Figure 3: z-component of the average electric field at aqueous interfaces. The geometry is defined in Fig 1

the solute needs to be simulated. Then, advantage is taken of the relationship between the excess chemical potential of the solute inserted into the system and the corresponding solute-solvent potential energy, U_{sol},

$$\Delta\mu_{exc} = -k_B T \ln < exp(-U_{sol}/k_B T) >_0, \tag{3}$$

where k_B is the Boltzmann constant, T is temperature and $< ... >_0$ signifies a thermal average over insertions into configurations of the system unperturbed by the solute. Here, we assume that the solute is rigid, a good approximation for the molecules considered in this paper. Furthermore, Eqn. 3 is exactly correct only for the NVT ensemble. In the NVE ensemble, a correction arising from temperature fluctuations should be included. (Frenkel and Smit, 1986) This correction becomes important near the critical temperature, but under conditions of the present simulations is expected to be small and, therefore, has been omitted.

Eqn. 3 simplifies greatly if the solute is a hard sphere (a cavity). Then, $exp(-U_{sol}/k_B T)$ is either 1 if the inserted hard sphere does not overlap with van der Waals spheres around solvent atoms or 0 otherwise and

$$\Delta\mu_{exc} = -k_B T \ln[P_{cav}(R)], \tag{4}$$

where $P_{cav}(R)$ is the probability of inserting a cavity of radius greater than or equal to R into the system. One efficient method of calculating $P_{cav}(R)$ has been proposed by Pohorille and Wilson, (Pohorille and Wilson, 1996) and the same method has been used in this work.

Once $P_{cav}(R)$ is known it can also be used as the probability density for inserting solute molecules. Then, Eqn. 3 takes the form:

$$\Delta\mu_{exc} = -k_B T \ln\left[\int_0^\infty P_{cav}(R) < exp(-U_{sol}/k_B T) >_R dR\right]. \quad (5)$$

where $< ... >_R$ represents a statistical overage over insertions of the solute into cavities with radii between R and $R + dR$.

Since $P_{cav}(R)$ is a rapidly decreasing function of R the efficiency of such a particle insertion method would be poor. Most cavity sites sampled from this distribution are too small to accommodate the solute, yielding very large U_{sol}, and, consequently, contribute practically nothing to the statistical average in Eqn. 5. However, the efficiency can be greatly improved by introducing a probability distribution, P_b, biased by a weighting function, $w(R)$, which increases with R:

$$P_b(R) = P_{cav}(R)w(R). \quad (6)$$

Then, $\Delta\mu_{exc}$ can be expressed as:

$$\Delta\mu_{exc} = -k_B T \ln\left[\int_{R_{min}}^\infty \frac{P_b(R)}{w(R)} < exp(-U_{sol}/k_B T) >_R dR\right], \quad (7)$$

where R_{min} is the smallest cavity size considered a suitable insertion site.

To calculate $\Delta\mu_{exc}$ as a function of z the system is divided into N layers of width Δz and the averaging in Eqn. 6 is carried out in each layer separately.

Calculations of $\mu_{exc}(z)$ start from configurations generated in molecular dynamics simulations of the neat interfacial system (without the solute). For each of these configurations a large number of solute insertions are made, governed by the probability distribution $P_b(R)$, and U_{sol} is evaluated at each insertion site. These potential energies are further used to estimate the statistical average in Eqn. 7.

A major advantage of the particle insertion method is that it may yield μ_{exc} of several different solutes at many different locations along z from a single simulation of the system in the absence of these solutes. This makes the method both highly efficient and accurate, a rare combination in computer simulations. The method, however, also has a major limitation — it is applicable only to atomic and small molecular solutes that can fit into voids that transiently form in the system. If the solute is too large, the number of sterically allowed insertions would be small and the accuracy of estimating μ_{exc} would suffer.

Excess chemical potentials of small solutes: In implicit models, the excess chemical potential of a solute molecule is commonly represented as a sum of two contributions — electrostatic and non-electrostatic — which are evaluated separately. The non-electrostatic term is usually obtained from empirical formulas for the reversible work required to create a cavity of appropriate size in the solvent, and for solute-solvent van der Waals interactions. In explicit models, the total excess chemical potential is calculated at once. Nevertheless, it is still possible to separate electrostatic and non-electrostatic terms by performing properly designed simulations. This is exactly the approach that we will follow. This approach not only may guide future developments of interfacial implicit models but also offers valuable insight into the origin of the observed profiles of $\Delta\mu_{exc}$.

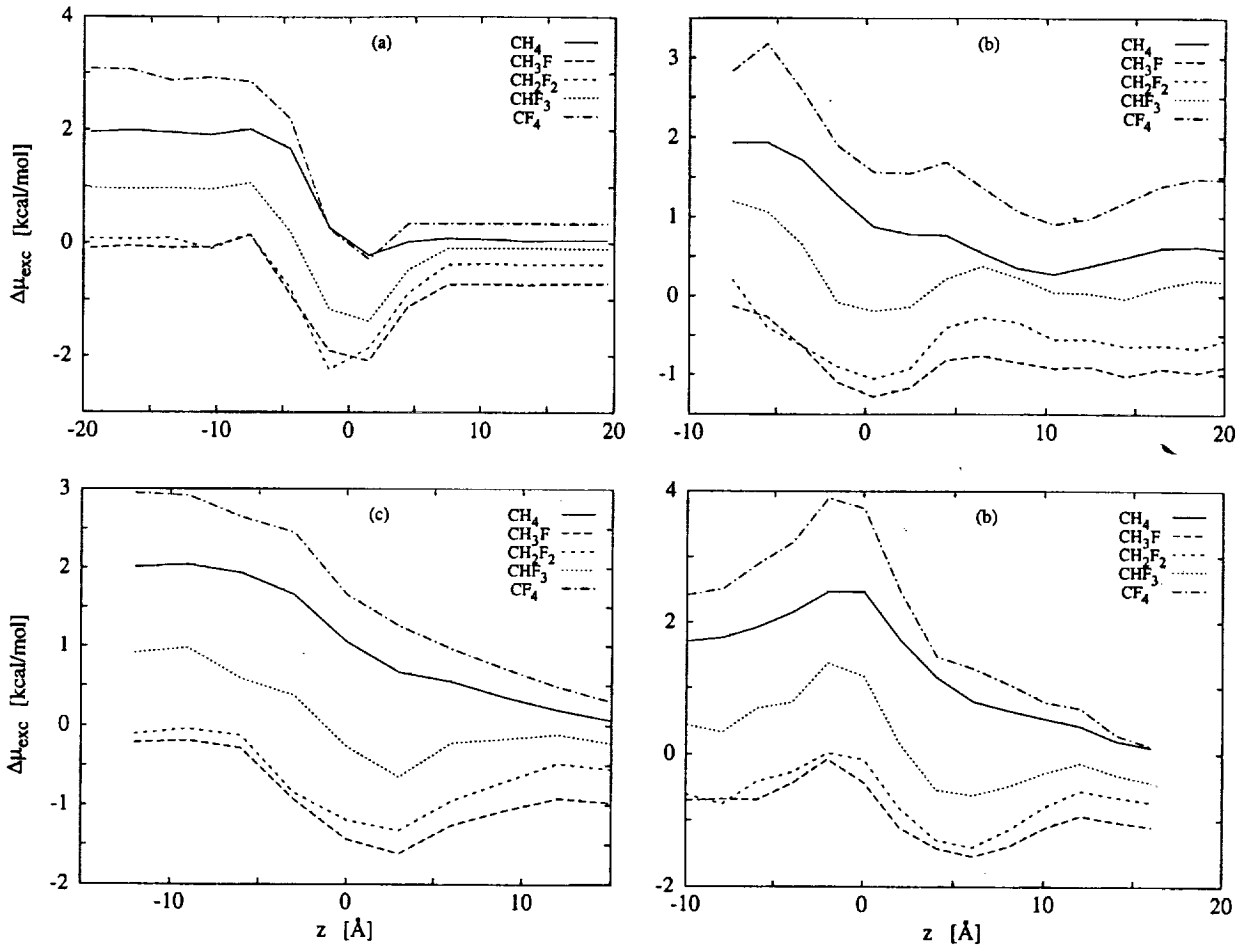

Figure 4: Excess chemical potentials of methane and its fluorinated derivatives across the (a) water-hexane, (b) water-octanol, (c) water-GMO, and (d) water-POPC interfaces. The geometry has been defined in Fig. 1.

First, we discuss the profiles of total $\Delta\mu_{exc}$, shown in Fig. 4. For the three dipolar fluoromethanes (CH_3F, CH_2F_2 and CHF_3) the profiles exhibit interfacial minima, indicating that these molecules tend to accumulate at the interface. The profiles, however, are not identical for all four interfacial systems. At the water-hexane interface, the minima are deeper (by approximately 1 kcal/mol) but not as broad as those at the water-GMO interface. The profiles in the water-octanol system reveal a lot of structure which is related to the extended layering of octanol in the interfacial region. However, due to difficulties in fully equilibrating octanol, it is uncertain whether the small features in these profiles away from the interface are statistically significant. For the water-POPC system, $\Delta\mu_{exc}$ exhibits not only a minimum, which is located on the hydrocarbon side of the head group region, but also a maximum on the water side of the interface. This feature is not present in the other three interfacial systems.

The profiles for nonpolar molecules, CH_4 and CF_4, are qualitatively different from the

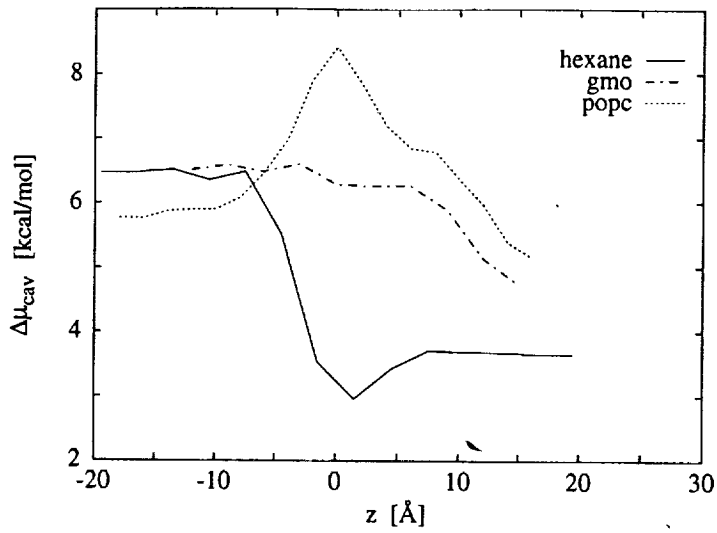

Figure 5: Excess chemical potential of cavity formation across the water-hexane, water-octanol, water-GMO, and water-POPC interfaces. The geometry has been defined in Fig. 1.

polar species. They exhibit a weak minimum at the water-hexane interface and no interfacial minima in the other three systems. $\Delta\mu_{exc}$ decreases monotonically or nearly monotonically across the water-octanol and water-GMO interfaces and exhibits a maximum at the water-POPC interface. A weak minimum in octanol separated from the interface by approximately one molecular layer reflects, again, interfacially induced ordering of octanol. In summary, in contrast to their polar analogs, nonpolar solutes concentrate in the organic phase or in the middle of the membrane bilayer.

The reversible work of cavity formation, μ_{cav}, which provides the main contribution to the non-electrostatic term, can be calculated from Eqn. 4 and the full non-electrostatic term can be obtained from Eqn. 3 by inserting into the solvent a hypothetical, nonpolar solute which has the same van der Waals parameters as the solute of interest but no distribution of partial charges. Then, the electrostatic term can be obtained by subtracting $\Delta\mu_{exc}$ of this hypothetical solute from $\Delta\mu_{exc}$ of the solute with the correct charge distribution.

In Fig. 5, we show $\mu_{cav}(z)$ for cavities of radius 2 Å across the four interfaces studied in this work. The most salient feature of these profiles is that they are non-monotonic in the interfacial region and change differently for different interfaces. Comparison between Figs. 1 and 5 reveals similarities between μ_{cav} and the mass density profiles for the corresponding interfaces. These similarities are not surprising. It is expected that it should be easier to insert a hard sphere in low mass density interfacial regions than in high mass density regions because they contain more free volume. The water-hexane interface serves as an example of such a region. In the water-octanol system, the minimum in $\mu_{cav}(z)$ is not located exactly at the interface, but instead in the low density tail region between the first and second layer of octanol. In contrast, when mass density reaches a maximum at the interface, as is the case

for the water-POPC system, we expect to find an interfacial maximum in $\mu_{cav}(z)$. It should be, however, kept in mind that this is only a qualitative argument and does not capture certain important structural features of solvents. For example, it has been shown that it is more difficult to insert a cavity of atomic or small molecular size into water than into other liquids even though they may have less free volume. (Pohorille and Pratt, 1990; Pratt and Pohorille, 1992). This is a reflection of the hydrophobic effect and it can be observed in Fig. 5 by comparing μ_{cav} on both sides of the interfaces and noting that it is always larger on the water side.

The inclusion of van der Waals interactions in $\Delta\mu_{exc}$ shifts the profiles of excess chemical potential towards lower values, but has little influence on their overall shape. Thus, in discussing the behavior of small, nonpolar species at different aqueous interfaces, we can be guided by $\mu_{cav}(z)$.

For other nonpolar molecules, profiles of $\Delta\mu_{exc}$ can take somewhat different shapes. One possible reason for such differences is that the reversible work of cavity formation may scale differently with cavity size in different regions along the z-direction. (Marrink *et al.*, 1996) Additionally, the ordering of phospholipid chains influences the shape of cavities. This is particularly evident in the region adjacent to the head groups. In this region finding a non-spherical cavity aligned with the lipid chains is considerably more probable than finding a spherical cavity with the same volume. (Bassolino-Klimas *et al.*, 1993; Marrink *et al.*, 1996)

The profiles for the electrostatic contributions, $\Delta\mu_{el}$, can be obtained by subtracting $\Delta\mu_{exc}$ for hypothetical solutes without partial atomic charges from $\Delta\mu_{exc}$ shown in Fig. 4. This approach was taken in the previous analysis of solutes at the water-hexane and water-GMO interfaces. (Pohorille and Wilson, 1996) This analysis, however, can be further clarified if, instead of the molecular solute, we consider a model solute consisting of a point dipole in the center of a cavity. This model is sufficiently simple that several useful results can be derived analytically. Simultaneously, as has been already shown (Pohorille and Wilson, 1996), $\Delta\mu_{exc}(z)$ for fluoromethanes can be faithfully reproduced by such a model if the cavity radius is properly chosen.

For the dipolar model, the solute–solvent electrostatic energy, U_{el}, is given as:

$$U_{el} = -\mathbf{p} \cdot \mathcal{E} = -p\mathcal{E}cos\theta, \tag{8}$$

where $\mathbf{p}$ is the dipole moment of the solute and $\mathcal{E}$ is the electric field created by the solvent and acting on the dipole and θ is the angle between these two vectors. Then, $\Delta\mu_{el}$, statistically averaged over dipolar orientations, is expressed as:

$$\Delta\mu_{el} = -k_BT \ln < e^{-U_{el}/k_BT} >_0 = -k_BT \ln < \frac{k_BT \sinh(p\mathcal{E}/k_BT)}{p\mathcal{E}} >_0 . \tag{9}$$

Here $< \ldots >_0$ represents a statistical average over configurations of the reference system (without the dipole).

In Fig. 6 we show interfacial profiles of $\Delta\mu_{el}$ for a 2.0 D dipole in a cavity the radius of which is 2 Å. The most striking feature of these profiles is that, within accuracy of the data, they are all quite similar. $\Delta\mu_{el}$ is constant in water, then increases approximately linearly in the interfacial region over a distance of 10 Å, and finally reaches a plateau of approximately

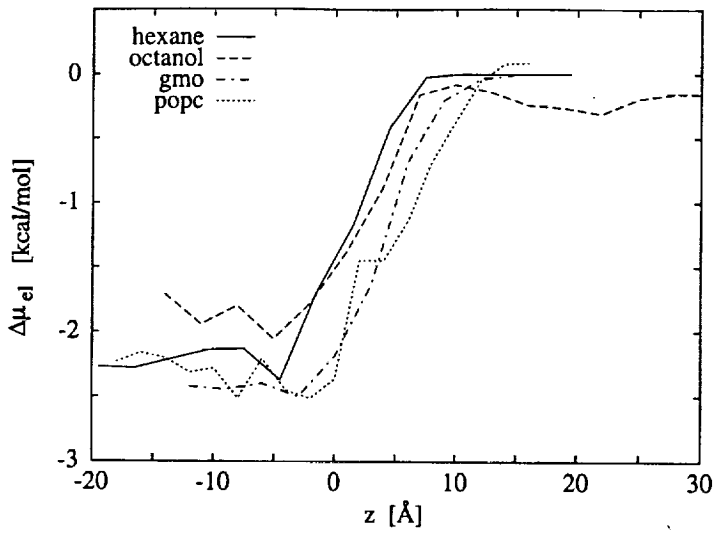

Figure 6: Electrostatic contribution to the excess chemical potential of a dipole of 2.0 D in a cavity of radius 2.0 Å across the water-hexane, water-octanol, water-GMO, and water-POPC interfaces. The geometry has been defined in Fig. 1.

zero in the bulk organic phase or inside the membrane bilayer. The shape or the width of the interfacially changing portion of the profile does not appear to depend significantly on the structure, polarity or ordering of chemical groups directly in contact with water.

Another issue of particular relevance in the context of developing successful implicit models is whether the linear response approximation is accurate at the interface. This requires that the second order perturbation theory for $\Delta\mu_{el}$ is satisfactory. In this approximation, $\Delta\mu_{el}$ is expressed as:

$$\Delta\mu_{el} = < U_{el} >_0 - \frac{k_B T}{2}[< U_{el}^2 >_0 - < U_{el} >_0^2] \tag{10}$$

Since $< U_{el} >_0$ averaged over dipolar orientations vanishes this expression simplifies to:

$$\Delta\mu_{el}(z) = -\frac{p^2}{6k_B T} < \mathcal{E}(z)^2 >_0 . \tag{11}$$

In the last formula we explicitly included the dependence on z to stress that $\Delta\mu_{el}$ changes with the distance from the interface.

Eqn. 11 implies that $\Delta\mu_{el}$ should be proportional to p^2 and, therefore, can be considered as a molecular-level equivalent of the well known Onsager formula obtained from the continuum model of bulk solvents. (Onsager, 1936). The dependence of $\Delta\mu_{el}$ on p^2 in bulk aqueous solution and in the interfacial regions is shown in Fig. 7. As can be seen, second order perturbation theory is quite accurate in water, but is less satisfactory at the water-hexane and water-octanol interfaces. Surprisingly, the linear relation between $\Delta\mu_{el}$ and p^2 appears to be well preserved at the water-POPC interface, despite large electric fields acting in this

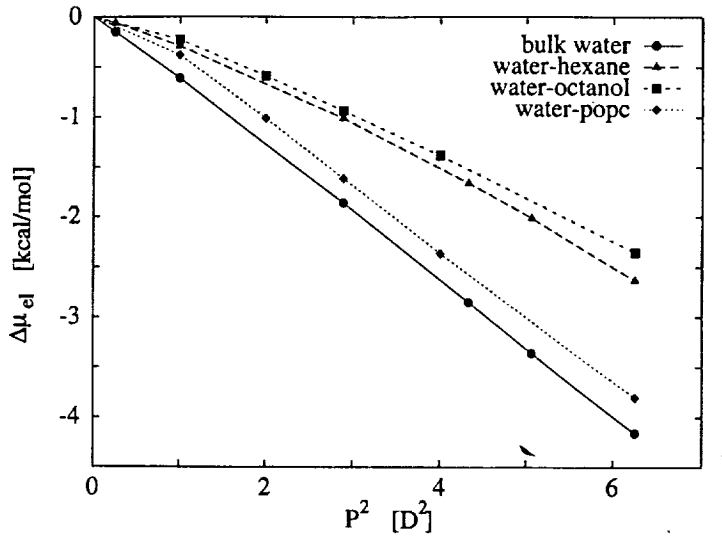

Figure 7: Electrostatic chemical potentials of dipoles in a cavity of radius 2 Å as a function of the square of the dipole moment in bulk water and at the water-hexane, water-octanol and water-POPC interfaces.

region. This may be a result of fortuitous cancelation of errors. Alternatively, it is possible that the accuracy of second order perturbation theory improves if long range effects are fully taken into account, as long-range interactions were only included in the water-POPC simulation.

Finally, we consider the orientational preferences of solutes at the interface induced by electric fields generated by the solvent. To this end, we examine point dipoles placed in a cavity and pointing parallel, antiparallel or perpendicular to the excess electric field, E_z, acting along the z-axis. The corresponding chemical potentials are $\Delta\mu_\uparrow$, $\Delta\mu_\downarrow$ and $\Delta\mu_\perp$, respectively. In the second order perturbation approximation they are expressed as:

$$\Delta\mu_\uparrow = -p < E_\parallel >_0 - \frac{p^2}{2k_BT}[< E_\parallel^2 >_0 - < E_\parallel >_0^2]$$

$$\Delta\mu_\downarrow = p < E_\parallel >_0 - \frac{p^2}{2k_BT}[< E_\parallel^2 >_0 - < E_\parallel >_0^2] \qquad (12)$$

$$\Delta\mu_\perp = -\frac{p^2}{2k_BT} < E_\perp^2 >_0$$

where $E_\parallel$ and $E_\perp$ are components of the instantaneous electric field acting on the dipole in the directions parallel and perpendicular to E_z.

If only the first order terms are considered, $\Delta\mu_{exc}$ of the dipole oriented parallel to E_z should decrease proportionally to the excess electric field at location z, $\Delta\mu_{exc}$ of the dipole oriented antiparallel should increase by the same value and $\Delta\mu_{exc}$ of the dipole oriented perpendicular should be unaffected by the electric field. In other words, if perturbation

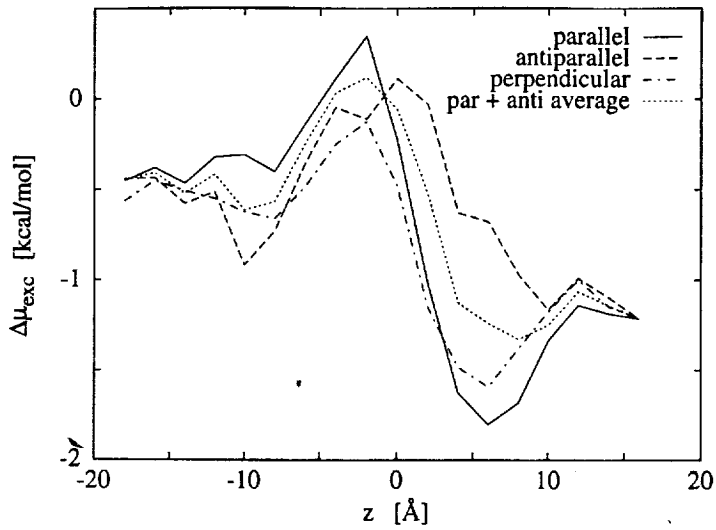

Figure 8: Excess chemical potentials of dipoles of 2.08 D in cavities of radius 2.0 Å oriented parallel, antiparallel and perpendicular to the interface across the water-POPC interface. The average of the excess chemical potentials of the parallel and antiparallel dipoles is also shown. The geometry has been defined in Fig. 1.

theory to first order is accurate, then the excess chemical potential of the perpendicular dipole should simply be the cavity free energy and the excess chemical potentials of the parallel and antiparallel dipoles should lie symmetrically below and above this value.

The corresponding numerical results for the water-POPC system are shown in Fig. 8. In the most general case, the electric field can change sign in the interfacial region, as we observed at the water-hexane interface (see Fig. 3), and the above notation would have to be generalized for orientations of dipoles that are fixed with respect to the interface. Since the electric fields at the water-POPC are of a single sign, to within our numerical accuracy, we retain the simpler notation. Although the lack of orientational averaging limits statistics and yields somewhat noisy profiles, certain features of these profiles are clear. First, dipoles at the interface tend to align themselves with the electric field. Second, the first order approximation captures the qualitative features of the profiles, and $\Delta\mu_{exc}$ of the dipole oriented parallel to the electric field lies below $\Delta\mu_{exc}$ of the dipole in the antiparallel orientation in most of the interfacial region. The average of $\Delta\mu_{exc}$ for the parallel and antiparallel dipoles has the same shape as $\Delta\mu_{exc}$ for the perpendicular dipole, but is consistently higher. This means that the second order term makes a significant contribution to the total chemical potential. It also indicates that fluctuations of the electric field are larger in the plane of the interface than in the perpendicular direction.

Organization of Peptides at Membrane Interfaces. We had previously studied the interfacial behavior of very short, model peptides and longer peptides composed of both polar and nonpolar amino acids. (Pohorille and Wilson, 1994a; Pohorille and Wilson, 1994b) All

these peptides exhibit interfacial activity, *i.e.* they tend to accumulate at aqueous interfaces. Recently, we extended these studies to the undecamer of poly-L-leucine at the water-hexane interface. Since this peptide consists only of nonpolar residues, it is not expected to be interfacially active but, instead, to partition into the nonpolar phase. Thus, our calculations consider a simple model of peptide insertion into the interior of a membrane, a phenomenon fundamental to the transduction of signals and the transport of material between the cell interior and the environment.

It is expected that most peptides composed of mixtures of polar and nonpolar residues will adopt amphiphilic, interfacially active structures. Whether these structures are ordered or not depends on the sequence of amino acids. In contrast, nonpolar peptides are expected to partition from water to a nonpolar medium. In aqueous solution, such peptides are disordered, whereas in nonpolar media, they most likely exist as α-helices. They must, therefore, fold during transfer across the interface. This is clearly relevant to the formation and insertion of transmembrane helices. A proposed scheme for this process is that integral peptides first accumulate at the water-bilayer interface and form the helix. (Jacobs and White, 1989) Once folded, the peptides penetrate the bilayer *via* the nonpolar regions of the α-helices. Alternative schemes, in which penetration precedes, or is coupled to, folding can also be envisioned.

We investigated these possibilities in the example of poly-L-leucine. First, we tested the predictions about its stability in water and hexane. When the undecamer was placed in water as a β-strand, it rapidly unfolded into a random coil — a family of disordered conformations observed during 6.2 ns of a molecular dynamics trajectory. The final structure was used in subsequent simulations as a model for the random coil. In contrast, when the peptide was place in hexane in a β-strand or a random coil conformation, it refolded into an α-helical structure within 3.0 and 3.7 ns, respectively. In both cases, the folding proceeded sequentially from the C-terminus.

To simulate poly-L-leucine at the water-hexane interface, the peptide, in a random coil conformation, was placed in water such that its center of mass was *ca.* 11 Å from the interface. Initially, the undecamer moved rapidly towards the interface, partitioning to the interface within 1 ns. This indicates that a strong average force attracts a nonpolar peptide to the nonpolar phase. Once the peptide reached the interface, it started slowly folding into an α-helix and, simultaneously, partitioning into hexane. These two processes appear to be closely coupled: some penetration into hexane is needed to initiate folding. Then, as the helical structure started forming, some hydrophilic atoms of the backbone became shielded from the aqueous environment. This made the peptide structure more hydrophobic, allowing for greater penetration into the nonpolar phase and promoting further folding. The correlation between the evolution of the folding of the backbone and the center-of-mass (COM) of the peptide are show in Figure 9. In the present study, folding was not sequential. First, six consecutive residues, from the N-terminus, formed a helical fragment. Subsequently, four residues, from the C-terminus, folded into a helix. Here, the term "helix" denotes the portion of the Ramachandran map, for which $-180 \leq \phi \leq 0$ and $-90 \leq \psi \leq 0$. After 34 ns, the completely formed helix was immersed in hexane, just next to the interface.

Folding of the peptide proceeded through an intermediate, a 3_{10}-helix. During the sim-

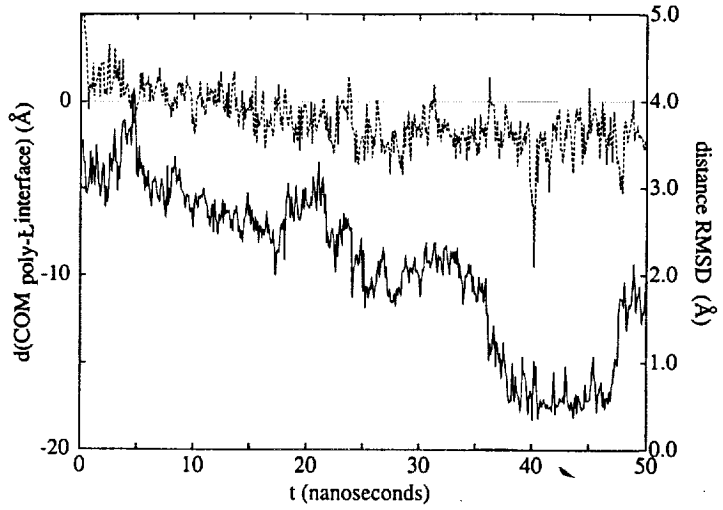

Figure 9: Position of the peptide center-of-mass (dotted line) and the deviation of the peptide backbone from an α-helix (solid) line as a function of time.

ulations, this helix persisted for only 2 ns before converting to the α-helix. The two helices differ in the pattern of hydrogen bonding along the peptide backbone. In an α-helix, each hydrogen bond involves residues separated by three other residues, whereas in a 3_{10}-helix the participating residues are separated by only two other residues. Occasional formation of the 3_{10}-helix was also observed for the folded peptide. This indicates that this helix not only mediates folding but remains in equilibrium with the α-helix once this process is completed. A very similar conclusions was reached from experimental studies of alanine-based peptides in aqueous solution.

The orientation of the peptide, defined by the direction of the end-to-end vector, is nearly parallel to that interface. However, orientations nearly perpendicular to the interface with the N-terminus buried in hexane are also probable. In contrast, perpendicular orientations with the C-terminus in hexane are highly unfavorable since they require dehydration of the three carbonyl group at this end of the peptide which are not involved in intramolecular hydrogen bonding. Most transmembrane proteins exhibit similar preferences and incorporate into the membrane through the N-terminus.

Since nonpolar peptides appear to adopt helical structures in nonpolar environments, independently of their specific sequence, we propose that inserting such peptides into nonpolar liquids and membranes requires simultaneous folding and penetration. Although results from a single trajectory are insufficient to draw general conclusions about the mechanism of folding, we note that nonsequential pathways are, at least, probable. Determining whether they are also the most preferred, and how equilibrium free energy and kinetic effects contribute to the selection of folding pathways, requires further studies.

Transport of ions across membrane interfaces. Simple ions, such as Na^+, K^+, Cl^- and Ca^{2+}, play an essential role in a wide variety of cellular processes, such as bioenergetics, intercellular signaling and the catalysis of chemical reactions. To enter cells, ions

must permeate their lipid membranes. There is a large free energy of activation associated with transferring a charged species from a polar environment to the nonpolar interior of a membrane. Thus, a membrane forms a permeability barrier to ions, making them excellent structures for mediating many cellular regulatory processes. In contemporary cells, ion transport is precisely controlled with the assistance of transmembrane ion channels, carriers and pumps located in membranes. However, to fully understand the transport of charges across membranes, it is necessary to begin with passive ion transport. Such uncontrolled transport is usually unproductive, and sometimes harmful to cells, but useful in artificial, membrane-bounded structures such as liposomes.

The permeation rate of ions across membranes can be estimated using a continuum dielectric model of a water-membrane system. In this model, both water and membrane are represented as homogeneous, isotropic media, characterized by dielectric constants ϵ_w and ϵ_b, respectively, and separated by a sharp planar boundary. If the ion is represented as a point charge q located at the center of a cavity of radius a, the change in the excess chemical potential associated with the transfer of the ion from bulk water to the center of the membrane (the free energy barrier), $\Delta\mu_{\text{exc}}^{\text{TS}}$, is expressed in this model as (Parsegian, 1969; Neumcke and Läuger, 1969):

$$\Delta\mu_{\text{exc}}^{\text{TS}} = \frac{q^2}{2a}\left[\frac{1}{\epsilon_b} - \frac{1}{\epsilon_w}\right] - \frac{q^2}{\epsilon_b w_m}\log\left(\frac{2\epsilon_w}{\epsilon_w + \epsilon_b}\right) \tag{13}$$

where w_m is the width of the membrane. For an ion with the effective radius of Na^+, $\Delta\mu_{\text{exc}}^{\text{TS}}$ is approximately equal to 47 kcal/mol. This yields a membrane permeability of 10^{-29} cm s^{-1}, approximately 17 orders of magnitude lower than the measured permeability of Na^+ (Wilson and Pohorille, 1996). This discrepancy is so large that it cannot be easily explained by uncertainties in the parameters of equation (13). Thus, the continuum dielectric model fails to accurately represent the energetics of ion transfer across biological membranes. The question is, why does it fail?

To help answer this question, a detailed, molecular simulation of the unassisted ion transport of Na^+ and Cl^- across a GMO bilayer was performed using molecular dynamics (Wilson and Pohorille, 1996). Due to the large free energy barrier, however, the transfer does not occur on the timescales accessible to computer simulations. Therefore, a series of molecular dynamics trajectories were generated in which the ion was restricted to overlapping regions along the interface normal (z-direction).

The simulations revealed a picture of ion permeation that is in sharp contrast with the continuum dielectric model. As the ion moves across the water-membrane interface into the bilayer, the membrane surface does not remain approximately planar. Instead, a local deformation is formed in which water molecules and polar head groups (normally restricted to the surface of the membrane) follow the ion into the nonpolar interior of the bilayer. Once the ion crosses the midplane of the membrane, the deformation on the incoming side relaxes and simultaneously, a similar deformation forms on the outgoing side. Thus, during the entire transfer process, the ion remains partially solvated by both the polar head groups and water molecules. The key feature of this *molecular* description of the ion transfer process is that the ion is never fully solvated by the nonpolar hydrocarbon tails. Thus, the calculated $\Delta\mu_{\text{exc}}^{\text{TS}}$

is markedly lower than the barrier predicted from the continuum model. For Na^+, $\Delta\mu_{exc}^{TS}$ was estimated at 27 kcal/mol. The full profile of $\Delta\mu_{exc}$ across the membrane is shown in Figure 10. The barrier for Cl^- was approximately 2 kcal/mol lower. To obtain this estimate it was necessary to correct for the absence of permanent and induced partial charges on the atoms of the GMO tails. The lack of charges would yield ϵ_b of the membrane interior equal to 1 instead of 2, as expected for real membranes (Ohki, 1968; Dilger *et al.*, 1982).

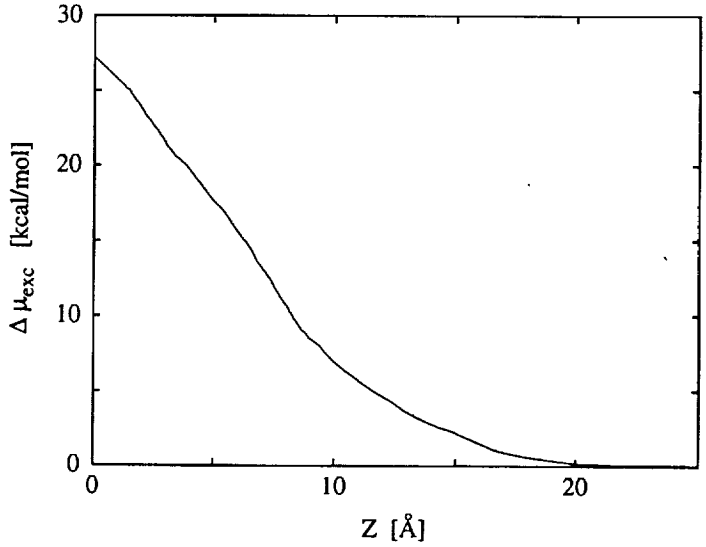

Figure 10: Free energies of transferring Na^+ across the water GMO interface. The center of the membrane is at $z = 0$.

Once $\Delta\mu_{exc}^{TS}$ is known, the permeability coefficient can be estimated by expanding $\Delta\mu_{exc}(z)$ in the high barrier limit (Wilson and Pohorille, 1996):

$$P_{membr} = \sqrt{\frac{\beta a}{\pi}} D_b \exp\left[-\beta \Delta\mu_{exc}^{TS}\right] \tag{14}$$

where $a = (1/2) \mid \partial^2 \Delta\mu_{exc}(z)/\partial z^2 \mid$ and D_b is the diffusion coefficient in the z-direction at the midplane of the bilayer.

The calculated P_{membr} for Na^+ is approximately 10^{-15} cm s^{-1}. This value is slightly lower than most experimental estimates for phospholipid bilayers (Hauser *et al.*, 1973; Nozaki and Tanford, 1981; Deamer and Volkov, 1995). Considering, however, that the error in the calculated $\Delta\mu_{exc}^{TS}$ is approximately 4 kcal/mol, corresponding to an uncertainty in P_{membr} of 3 orders of magnitude, the agreement between the simulated and measured permeabilities is satisfactory. The permeability coefficient for Cl^- , computed from the molecular dynamics simulations, is approximately 2 orders of magnitude higher than that for Na^+ , again in good agreement with experiment (Hauser *et al.*, 1973; Paula *et al.*, 1998). The difference in permeability between Na^+ and Cl^- most likely reflects the difference in μ_{exc} of these two ions in water. This, in turn, is associated with the larger ionic radius of Cl^-, properly adjusted

for a different orientation of water molecules around positive and negative ions (Rashin and Honig, 1985). As a result, partial desolvation accompanying the transfer of an ion from water to the membrane requires less free energy for Cl^- than for Na^+.

These simulations were performed only for one type of the membrane. Therefore, there is no direct data on the effect of different head groups and membrane widths on ionic permeability. It can be expected, however, that for sufficiently wide membranes, the formation of deep deformations, extending to the midplane of the bilayer, would become highly unfavorable. Then, the ion would have to undergo almost complete desolvation near the center of the bilayer. In that region, the change in $\Delta\mu_{\rm exc}^{\rm TS}$ may become similar to that predicted from the continuum dielectric model.

Conclusions

Computer simulation of several aqueous interfaces, from the simple water-hexane interface to the more densely packed water-POPC interface have show that the adsorption of small solutes at these interfaces can be understood as a balance between electrostatic effects and non-electrostatic terms. For polar solutes, the free energy arising from electrostatic effects decreases from the nonpolar phase to the water. On the other hand, the non-electrostatic term increases from the nonpolar phase to water. We find that the electrostatic term decreases sufficiently strongly to give rise to a free energy minimum at water-oil and water-membrane interfaces, indicating that small, polar solutes are adsorbed at these interfaces.

Separating the free energy into its electrostatic and non-electrostatic parts also highlights two important points. First, the variation in the electrostatic term in the interfacial region is similar for all the interfaces we have investigated. This suggests that it might be possible to build simple implicit theories to account for this term. Second, the non-electrostatic term is a sensitive function of the solvent density in the interfacial region. This term shows a free energy minimum at the water-hexane interface, where the hydrophobic phase is directly in contact with the aqueous phase. But this minimum disappears for the more densely packed amphiphilic, bilayer systems. This is a significant problem because it is not clear that it will be possible to extend theories of cavity formation, which have been well characterized for bulk phases, into the interfacial region.

The electric fields and free energy required to form cavities at the interface clearly influence the adsorption and and orientational and conformational equilibria of small solutes in the interfacial region. For larger molecules, such as peptides, the situation is more complex. If peptides consist of nonpolar residues only, they become inserted into the nonpolar phase. As demonstrated by the example of the leucine undecamer, such peptides fold into an α-helix as they partition into the nonpolar medium. The folding proceeds through an intermediate, called the 3_{10}-helix, which remains in equilibrium with the α-helix. This process represents a simple, protobiologically relevant example of environmentally-mediated self-organization of biological molecules. Once in the nonpolar environment, the peptides can readily change their orientation with respect to the interface from parallel to perpendicular, especially in response to local electric fields. The ability of nonpolar peptides to modify both the structure and orientation with changing external conditions may have provided a simple mechanism

of transmitting signals from the environment to the interior of a protocell.

While the free energy of cavity formation and the interfacial electric fields determine the permeability small polar solutes, they have a much smaller effect on the unassisted transport of ions across a membrane. In this case, it is the flexibility of the bilayer that determines the mechanism of ion transport across asymmetric thinning defects in the membrane. In this mechanism, the head groups on the incoming side of the bilayer follow the movement of the ion into the membrane interior by tilting inwards. The resulting defect is filled with water. Once the ion crosses the mid-plane of the bilayer, the defect on the incoming side of the membrane disappears and a similar deformation is formed on the outgoing side. During the transfer, the ion remains solvated by both head groups and water molecules. Even though the calculated ionic permeabilities are subject to considerable uncertainties, this mechanism qualitatively accounts for a large increase in these permeabilities (by 14-17 orders of magnitude), compared to the estimates from the rigid membrane model. Our results imply that the permeability of thin membranes to ions should change with the bilayer width more rapidly than expected from the continuum dielectric model, also in agreement with experimental results (Deamer and Volkov, 1995). This offers, for example, the possibility of regulating release of charged therapeutic agents from liposomes. The calculations also illustrate the broader point hat polar groups and/or molecules in the membrane can readily reorganize to stabilize a charge inside the bilayer. It is likely that this effect should be considered, for example, in the studies of the mechanism by which peptides with charged residues are incorporated into lipid bilayers.

Future Directions

One motif that is both appealing as a method of obtaining new functions from existing peptides and exists in many actual protein assemblies such as the superfamily of ligand-gated ion channels, is the aggregation of several peptides together to form a transmembrane assembly. Such an assembly could have functioned as a simple signaling system or as an ion transporter. We are investigating the free energetics and kinetics of the dimerization and insertion of the designed peptide, $(LSLLLSL)_3$, which forms tetrameric ion channels in the presence of an applied external voltage. Owing to the importance of proton transport across membranes throughout all living, cellular systems, we have initiated studies of a simple, proton-conducting, transmembrane channel to understand possible mechanisms of transport and gating.

References

Bassolino-Klimas, D., Alper, H.E., and Stouch, T.R. (1993). *Biochemistry* **32**, 12624–12637.

Benjamin, I. (1997). *Ann. Rev. Phys. Chem.* **48**, 407–451.

Cornell, W.D., Cieplak, P., Bayly, C.I., Gould, I.R., Merz, Jr., K.M., Ferguson, D.M., Spellmeyer, D.C., Fox, T., Caldwell, J.C., and Kollman, P.A. (1995). *J. Am. Chem. Soc.* **117**, 5179.

Deamer, D.W., and Volkov, A.G. (1995). *In* "Permeability and Stability of Lipid Bilayers" (E. A. Disalvo, and S. A. Simon, Eds.), pp. 161–177. CRC Press, Boca Raton.

Dilger, J.P., Fisher, L.R., and Haydon, D.A. (1982). *Chem. Phys. Lipids* **30**, 159–176.

Essmann, U., Perera, L., Berkowitz, M.L., Darden, T., Lee, H., and Pedersen, L.G. (1995). *J. Chem. Phys.* **103** , 8577–8593.

Frenkel, D., and Smit, B. (1986). "Understanding Molecular Simulations." Academic Press, San Diego.

Hauser, H., Oldani, D., and Philips, M.C. (1973). *Biochemistry* **12**, 4507–4517.

Jacobs, R. E., and White, S. H. (1989). *Biochemistry* **28**, 3421–3437.

Jorgensen, W.L., and Tirado-Rives, J. (1988). *J. Am. Chem. Soc.* **110**, 1657–1666.

Jorgensen, W.L., Chandrasekhar, J., Madura, J.D., Impey, R.W., and Klein, M.L. (1983). *J. Chem. Phys* **79**, 926–935.

Jorgensen, W.L., Madura, J.D., and Swenson, C.J. (1984). *J. Am. Chem. Soc.* **106**, 6638–6646.

Marrink, S.J., Sok, R.M., and Berendsen, H.J.C. (1996). *J. Chem. Phys.* **104**, 9090–9099.

Mitrinovic, D.M., Zhang, Z., Williams, S.M., Huang, Z., and Schlossman, M.L. (1999). *J. Phys. Chem. B* **103**, 1779–1782.

Neumcke, B., and Läuger, P. (1969). *Biophys. J.* **9**, 1160–1170.

Nozaki, Y., and Tanford, C. (1981). *Proc. Natl. Acad. Sci. USA* **78**, 4324–4328.

Ohki, S. (1968). *J. Theor. Biol.* **19**, 97–115.

Onsager, L. (1936). *J. Am. Chem. Soc.* **58**, 1486–1493.

Parsegian, V.A. (1969). *Nature* **221**, 844–846.

Paula, S., Volkov, A.G., and Deamer, D.W. (1998). *Biophys. J.* **74**, 319–327.

Pohorille, A. (1998). *In* "The Encyclopedia of Computational Chemistry" (N.L. Allinger, T. Clark, J. Gasteiger, P.A. Kollman, H.F. Schaefer, III, and P.R. Schreiner, Eds.), pp. 30–44. John Wiley & Sons, Chichester.

Pohorille, A., and Pratt, L.R. (1990). *J. Am. Chem. Soc.* **112**, 5066–5074.

Pohorille, A., and Wilson, M.A. (1993). *J. Mol. Struct. (Theochem)* **284**, 271–298.

Pohorille, A., and Wilson, M.A. (1994a). *In* "Structure and Reactivity in Aqueous Solution: Characterization of Chemical and Biological Systems" (C.J. Cramer, and D.G. Truhlar, Eds.). ACS Symposium Series No. 568, pp. 395–422. ACS, Washington D.C.

Pohorille, A., and Wilson, M.A. (1994b). *In* "Reaction Dynamics in Clusters and Condensed Phases" (C.J. Jortner, and *et al.*, Eds.). Kluwer Academic Publishers, the Netherlands.

Pohorille, A., and Wilson, M.A. (1996). *J. Chem. Phys.* **104**, 3760–3773.

Pohorille, A., Chipot, C., New, M., and Wilson, M.A. (1996). *In* "Pacific Symposium on Biocomputing '96" (L. Hunter, and T.E. Klein, Eds.), pp. 550–569. World Scientific, Singapore.

Pohorille, A., Wilson, M.A., Chipot, C., M.H., New., and Schweighofer, K.S. (1999). *In* "Computational Molecular Biology" (J. Lesczynski, Ed.). Theoretical and Computational Chemistry, pp. 485–526. Elsevier, Amsterdam.

Pratt, L.R., and Pohorille, A. (1992). *Proc. Natl. Acad. Sci. USA* **89**, 2995–2999.

Rashin, A.A., and Honig, B. (1985). *J. Phys. Chem.* **89**, 5588–5593.

Widom, B. (1963). *J. Chem. Phys.* **39**, 2808–2812.

Widom, B. (1982). *J. Phys. Chem.* **86**, 869–872.

Wilson, M.A., and Pohorille, A. (1994). *J. Am. Chem. Soc.* **116**, 1490–1501.

Wilson, M.A., and Pohorille, A. (1996). *J. Am. Chem. Soc.* **118**, 6580–6587.

Wilson, M.A., Pohorille, A., and Pratt, L. R. (1987). *J. Chem. Phys.* **88**, 3281–3285.

Zhang, Z., Mitrinovic, D.M., Williams, S.M., Huang, Z., and Schlossman, M.L. (1999). *J. Chem. Phys.* **110**, 7421–7432.

Publications Resulting from this Research

1. "Electrostatic Properties of Aqueous Interfaces Probed by Small Solutes," A. Pohorille, M. A. Wilson, and K. Schweighofer, in *Electrostatic Properties of Aqueous Interfaces Probed by Small Solutes*, L. R. Pratt and G. Hummer, eds., (AIP,1999) (in press).

2. "Interactions of small molecules and peptides with membranes," A. Pohorille, M. A. Wilson, C. Chipot, M. H. New, and K. Schweighofer, in *Theoretical and Computational Chemistry: Computational Molecular Biology* , J. Lesczynski, ed., (Elsevier, Amsterdam, 1999) pp. 485–526.

3. "Insights from computer simulations into the interactions of small molcules with membranes," A. Pohorille, M. H. New, K. Schweighofer and M. A. Wilson, in *Membrane Permeability: One hundred years since Ernst Overton (Current Topics in Membranes, Volume 48)*, D. Deamer, ed., (Academic Press, San Diego, 1999), Chapter 3, pp. 49–76.

4. "Folding and translocation of the undecamer of poly-L-leucine across the water-hexane interface. A molecular dynamics study," C. Chipot, and A. Pohorille, *J. Am. Chem. Soc.*, **120**, 11912 (1998).

5. "Conformational equilibria of terminally blocked single amino acids at the water-hexane interface. A molecular dynamics study," C. Chipot, and A. Pohorille, *J. Phys. Chem. B*, **102** 281 (1998).

6. "Structure and dynamics of small peptides at aqueous interfaces - A multi-nanosecond molecular dynamics study," C. Chipot, and A. Pohorille, *Theochem - J. Mol. Struct.*, **398** 529 (1997).

7. "Adsorption and Solvation of Ethanol at the water liquid-vapor interface," M. A. Wilson and A. Pohorille, *J. Phys. Chem.*, **101**, 3130 (1997).

8. "Interactions of Alcohols and Anesthetics with the Water-Hexane Interface: a Molecular Dynamics Study," A. Pohorille, M. A. Wilson, and C. Chipot, in *Progress in Colloid and Polymer Science*, **103**, 29 (1997).

9. "Mechanism of Unassisted Ion Transport across Membrane Bilayers," M. A. Wilson and A. Pohorille, *J. Am. Chem. Soc.*, **118**, 6580 (1996).

10. "Excess chemical potential of small solutes across water-membrane and water-hexane interfaces," A. Pohorille and M. A. Wilson, *J. Chem. Phys.*, **104**, 3760 (1996).

11. "Molecular Modeling of Protocellular Functions," A. Pohorille, C. Chipot, M. H. New, and M. A. Wilson, *Proceedings of the Symposium on the Evolution of Molecular Structures and the Structure of Molecular Evolution*, L. Hunter and T. E. Klein, eds. (World Scientific, Singapore, 1995) pp. 550-569.

12. "Scattering of water from the glycerol liquid-vapor interface," I. Benjamin, M. A. Wilson, A. Pohorille, and G. N. Nathanson, *Chem. Phys. Lett.*, **243**, 222 (1995). *Astrophysical Journal*, **455**, 389 (1995).

13. "Molecular dynamics studies of simple membrane-water interfaces: structure and functions in the beginning of cellular life," A. Pohorille and M. A. Wilson, *Orig. Life and Evol. Biosphere*, **25**, 21 (1995).

Invited Presentations from this Research

1. "Molecular Simulations of Protocellular Membrane Functions," **Andrew Pohorille**, Michael A. Wilson, Karl Schweighofer, Christophe Chipot, and Michael H. New, The 9th ISSOL Meeting and the 12th International Conference on the Origin of Life, San Diego, July 11–17, 1999.

2. "Electrostatic Properties of Interfaces between Water and Hexane, Octanol and Membranes Probed by Small Solutes," **Andrew Pohorille**, Karl Schweighofer, and Michael A. Wilson, Workshop on Treatment of Electrostatic Interactions in Computer Simulations of Condensed Media, Santa Fe, NM, June 23–25, 1999,

3. "Interaction of Small Solutes with Aqueous Interfaces," **Michael A. Wilson** and Andrew Pohorille, Mesilla Chemistry Workshop on Kinetics, Dynamics and Thermodynamics at Interfaces, Mesilla, NM, February 7–10, 1999.

4. "Molecular Modeling Of Protocellular Structures And Functions," **Andrew Pohorille**, Michael A. Wilson, Michael H. New, and Christophe Chipot, 6th Symposium on Chemical Evolution and the Origin and Evolution of Life, Moffett Field, CA, November 17–20, 1997.

5. "Molecular Dynamics of Peptide Folding at Aqueous Interfaces," **Andrew Pohorille** and Christophe Chipot, 214th American Chemical Society Meeting, Las Vegas, NV, September 7–11, 1997.

6. "Adsorption and Solvation of Ethanol at the Water Liquid-Vapor Interface: a Molecular Dynamics Study," **Michael A. Wilson** and Andrew Pohorille, 214th American Chemical Society National Meeting, Las Vegas, NV, September 7–11, 1997.

7. "Uptake of Solutes by Aqueous Interfaces," **Michael A. Wilson** and Andrew Pohorille, Gordon Research Conference on Chemistry at Interfaces, Meridan, New Hampshire, July 21–26, 1996.

8. "Structure and Functions of Simple Peptides at Membrane-Water Interfaces," Christophe Chipot and **Andrew Pohorille**, The 8th ISSOL Meeting and the 11th International Conference on the Origin of Life, Orleans, France, July 7–12, 1996,

9. "Adsorption of Small Molecules at Water-Hexane and Water-Membrane Interfaces," **Michael A. Wilson**, Christophe Chipot and Andrew Pohorille, American Physical Society March Meeting, St. Louis, MO, March 18-22, 1996.

10. "Interactions of Anesthetics and Alcohols with the Water-Hexane Interface," **Michael A. Wilson**, Christophe Chipot and Andrew Pohorille, American Chemical Society National Meeting, Chicago, IL, August 20-24, 1995.

11. "Computer Simulations of Transport across Aqueous Interfaces: Implications in the Origins of Life," **Michael A. Wilson** and Andrew Pohorille, Planetary Biology Seminar, NASA Ames Research Center, Moffett Field, CA, August 3, 1995.

12. "Molecular Microenvironments: The Structure and Functions of Protocells," **Michael A. Wilson** and Andrew Pohorille, Exobiology Program Review, NASA Ames Research Center, Moffett Field, CA, April 25, 1995.